Spectrochimica Acta Part A: Molecular and Biomolecular Spectroscopy 298 (2023) 122792

Contents lists available at ScienceDirect

Spectrochimica Acta Part A:
Molecular and Biomolecular Spectroscopy

journal homepage: www.journals.elsevier.com/spectrochimica-acta-part-a-molecular-and-biomolecular-spectroscopy

Considerations on chemical composition of psammoma bodies: Automated detection strategy by infrared microspectroscopy in ovarian and thyroid cancer tissues

Francesco Porcelli [a], Martina Verri [b], Serena De Santis [a], Anna Crescenzi [b], Antonella Bianchi [b], Anna Candida Felici [c], Giovanni Sotgiu [a], Susanna Romano [a], Monica Orsini [a,*]

[a] Department of Industrial, Electronic and Mechanical Engineering, Roma Tre University, Via Vito Volterra 62, 00146 Rome, Italy
[b] Pathology Unit, University Hospital Campus Bio-Medico, Rome, Italy
[c] Basic and Applied Sciences for Engineering, Sapienza University, Via A. Scarpa 16, Rome, Italy

HIGHLIGHTS

- The chemical composition of psammoma bodies in ovarian serous tumors was obtained.
- The main component found by IR analysis is amorphous carbonated calcium phosphate.
- Na, Mg, Cu and Zn revealed in psammoma bodies as possible indicators of malignancy.
- Psammoma bodies automatic recognition in ovarian and thyroid cancer was performed.

GRAPHICAL ABSTRACT

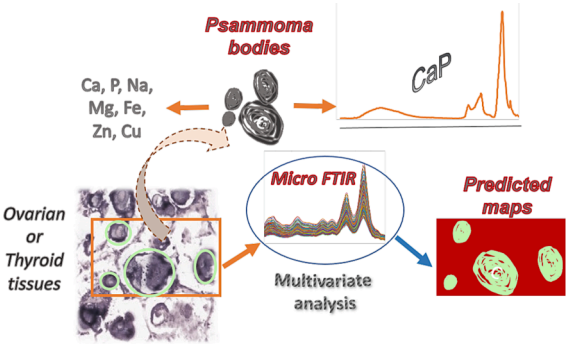

ARTICLE INFO

Keywords:
Psammoma bodies
Human ovarian serous tumor
Micro-FTIR spectroscopy
Chemical compositions
Automatic recognition

ABSTRACT

Ectopic calcifications are observed in many soft tissues and are associated with several diseases, including cancer. The mechanism of their formation and the correlation with disease progression are often unclear. Detailed knowledge of the chemical composition of these inorganic formations can be very helpful in better understanding their relationship with unhealthy tissue. In addition, information on microcalcifications can be very useful for early diagnosis and provide insight into prognosis. In this work the chemical composition of psammoma bodies (PBs) found in tissues of human ovarian serous tumors was examined. The analysis using Micro Fourier Transform Infrared Spectroscopy (micro-FTIR) revealed that these microcalcifications contain amorphous calcium carbonate phosphate. Moreover, some PB grains showed the presence of phospholipids. This interesting result corroborates the proposed formation mechanism reported in many studies according to which ovarian cancer cells switch to a calcifying phenotype by inducing the deposition of calcifications. In addition, other techniques as X-ray Fluorescence Spectroscopy (XRF), Inductively Coupled Plasma Optical Emission Spectroscopy (ICP-OES) and Scanning electron microscopy (SEM) with Energy Dispersive X-ray Spectroscopy (EDX) were performed on

* Corresponding author.
E-mail address: monica.orsini@uniroma3.it (M. Orsini).

https://doi.org/10.1016/j.saa.2023.122792
Received 14 January 2023; Received in revised form 4 April 2023; Accepted 25 April 2023
Available online 1 May 2023

the PBs from ovary tissues to determine the elements present. The PBs found in ovarian serous cancer showed a composition comparable to PBs isolated from papillary thyroid.

Based on the chemical similarity of IR spectra, using micro-FTIR spectroscopy combined with multivariate analysis, an automatic recognition method was constructed. With this prediction model it was possible to identify PBs microcalcifications in tissues of both ovarian cancers, regardless of tumor grade, and thyroid cancer with high sensitivity. Such approach could become a valuable tool for routine macrocalcification detection because it eliminates sample staining, and the subjectivity of conventional histopathological analysis.

1. Introduction

Ectopic calcifications are present in many soft tissues and these unexpected formations are associated with different diseases [1]. Nevertheless, the genesis of these pathological inorganic materials is still highly debated, and it represents an attractive scientific challenge [2]. Many aspects of biomineralization have been studied, including chemical composition, mineral content, nature of the crystals present and involvement of tissue components, in order to clarify the correlation between these formations and the progression of a specific disease [3]. Moreover, a thorough understanding of such pathological calcifications could allow them to be used in the diagnosis and prognosis of diseases [4].

Pathological calcifications are particularly heterogenous and can be related to different diseased conditions including several types of tumors [5]. The various types of microcalcifications observed include Psammoma Bodies (PBs) which are concentric lamellar round structures ranging from 20 to 100 μm in diameter [6]. Their occurrence has been found in a wide variety of benign and malignant conditions [7–9], but because of the possible association with an underlying malignancy, the study of these microcalcifications is particularly important [10]. Among the malignancies described in association with PBs, the most frequent are papillary thyroid carcinoma [11], meningioma [12], and serous tumors of the ovary[13]. Different pathways of mineralization have been reported for PBs formation, but the issue remains controversial [6,14]. Some proposed mechanisms focus on cell necrosis, as calcium accumulation is known to occur within necrotic tissues [15]. Other suggested pathways consider PBs as the result of active processes. Based on these hypotheses, some components of the extracellular matrix, which are found to be involved in physiological bone formation, appear to participate in the formation of PBs [5,6]. In this regard, a careful chemical characterization of PBs could provide insights into the mineralization mechanism leading to formation of PBs. In addition, the chemical knowledge gained about such microcalcifications could be exploited as robust tools for an early diagnosis of associated diseases.

In this work, chemical composition of PBs present in surgical samples from patients with high-grade serous carcinoma of the ovary were determined. In order to obtain a complete and comprehensive chemical characterization of these microcalcifications, various techniques were used, and different kind of samples were examined. Micro Fourier Transform Infrared Spectroscopy (micro-FTIR), X-ray fluorescence spectroscopy (XRF) and Inductively Coupled Plasma Optical Emission Spectroscopy (ICP-OES) were employed to analyze samples of PBs isolated from tissues and Scanning Electron Microscopy (SEM) with Energy Dispersive X-ray Spectroscopy (EDX) imaging to explore tissue samples containing PBs.

In our previous paper, the chemical nature of thyroid calcifications was carefully analyzed [16], and comparison with the results obtained for PB in ovaries revealed many similarities. In particular, it was observed that the IR spectra of PBs isolated from the two different tumor tissues were highly comparable. Based on this chemical similarity, by using micro-FTIR in conjunction with multivariate analysis, an automated recognition method of PBs in both cancer tissues was constructed. This technique, which combines microscopy and infrared spectroscopy, provides infrared maps of the analyzed sample, in which each pixel contains an IR spectrum with biochemical information at each wavenumber. IR maps can be subjected to multivariate cluster analysis to obtain digitally colored images highlighting the different components of the tissue [17].

Here, the clustering analysis was applied to spectral data of ovarian serous carcinoma samples from patients with high-grade tumor. Based on the clustering results, the Partial-Least-Square Discriminant Analysis was applied to build a rigorous recognition model. The robustness of the prediction model was checked by using unknown tissue samples, from patients with high-grade, low-grade and borderline ovary tumors and with papillary thyroid carcinoma.

The proposed method is noninvasive, nondestructive, and does not require special preparation or staining of the analyzed tissues [18]. In addition, an interesting aspect is the automation of the procedure, which can reduce human involvement and provide an objective chemistry-based diagnostic strategy.

2. Materials and methods

2.1. Sample preparation

Grains of Psammoma bodies. Several samples of PBs were extracted from human ovary tissues surgically removed after sonographic evidence of ovarian mass and/or cytological diagnosis on abdominal effusion of high-grade serous carcinoma. Isolation process was performed under stereomicroscopy (Leica EZ4) using post-diagnosis formalin fixed residual tissue. The isolated materials were washed with ethanol, air dried and used for analysis (FTIR spectroscopy, XRF and ICP-OES) without any further chemical treatment.

Tissue slices containing Psammoma bodies. Tissue samples were obtained from formalin-fixed paraffin-embedded surgically removed specimens from 10 patients. Eight patients were diagnosed with serous tumors of different grade (high- and low-grade carcinomas and borderline tumors) [19] and two patients were diagnosed with papillary thyroid carcinoma [20]. Paraffin sections of 10 μm obtained from representative paraffin blocks were mounted on gold coated microscope slides, dewaxed in xylene, washed in absolute ethanol and air dried prior to be examined under FTIR microscope. For each sample, representative areas were selected, microscope images were captured, and corresponding IR maps were recorded.

Paraffin sections from high grade ovary serous carcinoma used in SEM-EDX analysis were obtained following the same procedure cutting, in this case, at a thickness of 30 μm.

All the materials and solvents used in this work were purchased from Merk Life Science (Milano, Italy) and used as received.

The study was conducted in accordance with the 1964 Helsinki Declaration and later amendments.

2.2. Optical microscopy

The optical microscope images of psammoma bodies collection were collected using a NB50TS trinocular light microscope equipped with a 6MP camera, zoom range (8x – 50x), LED illumination B2-1525 additional objective 2x.

2.3. X-ray fluorescence spectroscopy (XRF)

XRF measurements were carried out by using a spectrometer operating in air. The spectrometer was equipped with the X-ray generator Amptek MiniX (rhodium anode target, 127 μm beryllium window) and the Peltier cooled silicon drift detector Amptek 123-SDD (surface 25 mm^2, thickness 450 μm, 12.7 μm beryllium window). The energy resolution was 140 eV, full width half maximum at 5.9 keV. The incident and the revealed beams formed an angle of 45° with respect to the surface of the sample holder. This latter was constituted by a sheet of Japanese paper suspended at 3 cm from the X-ray generator anode and 3.5 cm from the detector surface. The X-ray generator was equipped with a 2 mm diameter collimator and was powered with an accelerating potential difference of 38 kV and an electronic current of 80 μA. The acquisition time was 600 s. In order to eliminate any possible contribution due to the sample holder a spectrum acquired on the Japanese paper was subtracted from the one acquired on the sample.

2.4. Inductively coupled plasma optical emission spectroscopy (ICP-OES)

2.4 mg of the grains of PBs collection was added to 10 ml of HNO_3 (3.25% w/w) and the mixture was heated at 100 °C for 48 h. The obtained homogeneous solution was filtered (0.22 μm, KAIRO Safe) and diluted 1:10. The solution and the blank were analyzed by ICP-OES *(iCAP™ 7200, Thermo Scientific)*. The accuracy of the analysis was checked by concurrent analysis of standard references.

2.5. Scanning electron microscopy (SEM) with energy dispersive X-ray spectroscopy imaging (EDX)

Detailed microstructural and compositional observation of PBs in human ovarian serous carcinoma tissue was obtained by SEM-EDX using a Zeiss Gemini SIGMA 300 FEG SEM equipped with Bruker EDX. 30 μm thick slices were deposited on golden slides and observed without any metallization. EDX analyses were performed at 20 kV of accelerating voltage, back scattered detector and working distance 7.5 mm.

2.6. Micro-Fourier transformed spectroscopy (micro-FTIR)

A Nicolet iN10 infrared microscope (Thermo Fisher) equipped with a Mercury-Cadmium-Telluride (MCT-A) nitrogen-cooled detector was used. FTIR spectra were collected in the 4000 – 650 cm^{-1} range with a spectral resolution of 4 cm^{-1}. Sixty-four (64) interferograms were averaged per spectrum and apodized using a Blackman-Harris correction. Data acquisition and spectra elaboration was carried out with the OMNIC SPECTA software provided by Thermo Fisher Scientific.

2.6.1. Analysis of isolated psammoma bodies

The spectra were acquired in ATR mode. The background spectrum was collected on air. Using the OMNIC SPECTA software, spectra were treated for atmospheric compensation to eliminate water vapour and CO_2 contributions. Moreover, baseline correction and smoothing with a Savitzky-Golay filter of 2nd order and width 11 points were applied.

2.6.2. Analysis of tissue samples

The spectra were acquired in reflection mode. Maps were recorded using a 15 × 15 μm^2 aperture and a step size of 15 μm, both on the × and y axis, with a spectral resolution of 4 cm^{-1}. A background spectrum was collected on a tissue-free area on gold coated microscope slides before any map acquisition. A minimum of 25 to a maximum of 56 spectra for × and/or y direction were acquired.

2.6.2.1. Data pre-processing. To exclude low intensity signal by data analysis, a minimum pass-filter was applied to raw-data following procedure described in previous work [21], considering a threshold of 100 as signal to noise ratio. Spectra excluded by the filter was set as NaN (Not a Number) in data matrix. Second derivative Savitzky-Golay filter with polynomial order of 3 and 11 points as frame-length was applied to raw data.

2.6.2.2. Clustering analysis. Unsupervised, Fuzzy c-means (FCM) clustering analysis was applied on pre-processed spectra for PBs identification. In FCM each pixel of the map is encoded based on their cluster membership probability, thus each spectrum can be assigned to multiple clusters with a cluster participation from 0 to 1. A number of clusters varying from 2 to 3 with fuzzy's index of 1.5 was used to separate PBs by organic environment.

2.6.2.3. Principal component analysis (PCA). Principal component analysis (PCA) analysis was performed on pre-processed spectra in the 1800–800 cm^{-1} spectral range. Variables in the original data set are reduced to smaller number of orthogonal variables called the principal components (PCs). The scores report the contribution of each spectrum related to the selected principal component and the corresponding loadings show which wavenumber is responsible for such contribution.

2.6.2.4. Partial-least-square discriminant analysis (PLS-DA). The initially Fuzzy c-means clustered spectra from ovarian tissue samples of two different patients were used to build the prediction model. Spectra with a probability of membership greater than 0.8 associated to cluster 1 and cluster 2, corresponding to PBs and organic environment, respectively, were collected into two separate classes and employed as training set for the PLS-DA prediction model. This model was constructed using three latent variables established through venetian blind cross validation. The selection of the number of VLs was based on the lowest cross-validation error rate in classification (Fig. S1) [22].

After testing the robustness of the PLS-DA model in internal validation using 10-fold venetian blind cross validation [23], the prediction model was applied on maps recorded from unknow ovarian and thyroid tissues obtained by eight different patients (6 with ovarian cancer and 2 with thyroid cancer). Classification results were presented as chemical color-coded images in which pale green pixels represent psammoma bodies, dark red pixels correspond to organic tissue and blue pixels correspond to tissue-free regions generated during sample preparation. PLS-DA was performed with Classification toolbox for MATLAB v5.4 [24].

3. Results and discussion

3.1. Chemical composition of ovarian psammoma bodies

3.1.1. FTIR spectroscopy

Psammoma bodies from human ovarian tissues, surgically removed after sonographic evidence of ovarian mass and/or cytological diagnosis on abdominal effusion of high-grade serous ovarian carcinoma, were isolated and analyzed after dehydration. Some grains of the obtained samples were observed with an optical microscope (Fig. 1a) and showed the typical appearance of inorganic formations (Fig. 1a). The collection of isolated PBs shown in Fig. 1a was analyzed using infrared spectroscopy in ATR mode and the average spectrum of several spectra recorded on different grains is reported in Fig. 1b. In this spectrum the main band at 1022 cm^{-1} is related to asymmetric PO_4^{3-} stretching mode while the symmetric stretching vibration of this group at 963 cm^{-1} appears as a shoulder (highlighted applying second derivative, Fig. S1). The signals at 1453, 1412 cm^{-1} and 871 cm^{-1} are associated with vibrations of CO_3^{2-} group. The broad signal around 3250 cm^{-1} and the band at 1640 cm^{-1} point out the presence of absorbed water. Based on the recorded signals these microcalcifications are composed of amorphous calcium carbonate phosphate. Indeed, the presence of the shoulder in the absorption band at 1022 cm^{-1} can be used as a fingerprint to confirm the presence of the

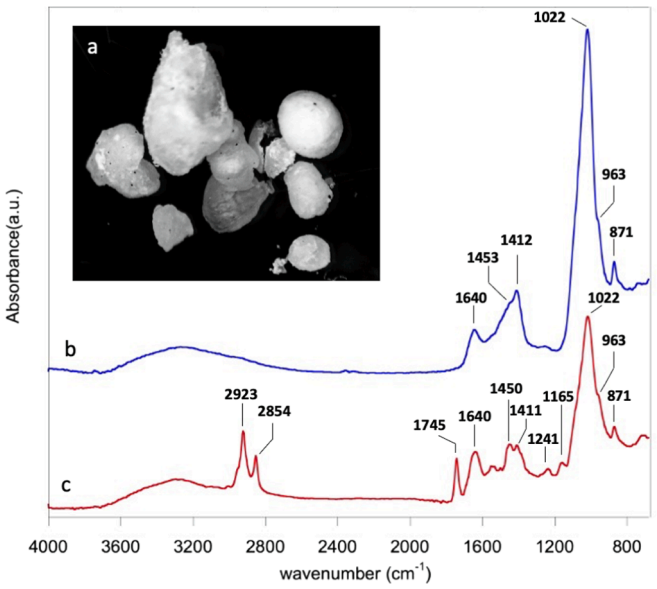

Fig. 1. (a) Light microscope image of white grains obtained from ground specimens extracted from ovarian serous carcinoma tissue containing many psammoma bodies microcalcifications. (b and c) Micro-FTIR average spectrum of representative sample shown in image a.

amorphous calcium carbonate phosphate compound [25]. Moreover, the bands at 1453 and 1412 cm^{-1} indicate the predominant presence of B-type carbonate, where CO_3^{2-} replaced PO_4^{3-} in the structure of PBs, rather than A-type carbonate, where CO_3^{2-} ions replaced OH^- ions [26]. Substitution of CO_3^{2-} at the B site reduces the crystallinity of calcifications [27], and this is further evidence that PBs from ovarian tissues are formed by amorphous calcium carbonate phosphate. This inorganic material is distinctive of malignant microcalcifications, whereas benign microcalcifications are generally formed by oxalates [5]. In addition, the structure of B-type carbonate more easily allows cations other than calcium to be included in these calcifications [27]. These results were in agreement with the spectra of ovary PBs reported in literature [28] but most importantly they further confirmed that these microcalcifications have a strong chemical and crystalline similarity to PBs isolated in thyroid cancer investigated in a previous work [16].

A small number of spectra randomly acquired from various grains (Fig. 1a) showed the presence of other signals in addition to those characteristics of amorphous calcium carbonate phosphate (Fig. 1c). These bands could be associated with biomolecules such as phospholipids. In fact, the strong band at 1745 cm^{-1} appears to be typical of the stretching of the ester carbonyl groups (C=O), while the signals at 3000–2500 cm^{-1} could derive from the methylene (CH_2) stretching vibrations. The other bands at 1450, 1241 and 1165 cm^{-1} could correspond to the CH_2 bending vibration mode, overlapping of the C-O and symmetric PO_2^- stretching, and antisymmetric stretching of PO_2^- respectively [29,30].

The possibility of detecting the presence of lipids in ovarian pathological calcifications using infrared spectroscopy analysis would help elucidating the process that leads to the formation of such microcalcifications. In particular, the presence of such biomolecules may support one of the recently proposed mechanisms by which ovarian cancer cells switch to a calcifying phenotype during disease progression. These cells induce the deposition of calcifications through processes mimicking physiological bone formation, in which matrix vesicles [31] consisting mainly of phospholipids are the primary site of mineralization [32].

3.1.2. X-ray fluorescence spectroscopy (XRF), inductively coupled plasma optical emission spectroscopy (ICP-OES) and scanning electron microscopy (SEM) with energy dispersive X-ray spectroscopy imaging (EDX)

In order to achieve an exhaustive chemical characterization of ovarian PBs, both the XRF and the ICP-OES analysis were performed on isolated granules. In particular, ICP-OES analysis was applied to investigate the presence of specific elements that were shown to be involved in the tumorogenesis and progression of ovarian cancer [33]. In addition, the Scanning Electron Microscopy with energy dispersive X-ray Spectroscopy Imaging was carried out on calcifications within tissues. This technique made it possible to find the elemental distribution in the analyzed sample area, providing spatial information about the elements contained in the microcalcifications. Using these techniques, comprehensive information related to elemental composition of these microcalcifications was obtained.

The elements Ca, P, S, K, Fe, Zn and Sr were detected using XRF (Fig. 2a) carried out on sample grains shown in Fig. 1a. Calcium and phosphorous have confirmed that these microcalcifications are mainly composed of calcium phosphate, while the other metal elements such as iron, zinc and strontium probably replaced a small part of the calcium cations of inorganic matrix. These findings are in agreement with several studies where it was reported that the amount of iron increases in diseased tissues since it plays a crucial role in tumor progression [34]. In addition, an increase in both Zn and Cu was observed in gynecological neoplasms and it was reported that these elements may influence carcinogenesis, considering their significant role in oxidative stress and chronic inflammation [35]. To evaluate if this element can also be included within ovarian PBs in cancer progression, ICP-OES analysis of a portion of grains was performed. In fact, ICP-OES allows a very low detection limit. This analysis disclosed the presence of copper and in addition confirmed that the macrocalcifications contain iron and zinc (Table S1).

The analysis by SEM of ovarian cancer tissue allowed the identification of typical psammoma bodies as shown in Fig. 2b. The EDX imaging investigation was performed in the selected region within microcalcifications, to reveal the contained elements and their distribution. The corresponding microanalysis spectrum (Fig. 2c) and the element maps (Fig. 2d) pointed to the presence of carbon, oxygen, calcium, phosphorous, magnesium and sodium. Calcium and phosphorous have already been revealed through the XRF applied on isolated PBs. The high levels of these elements, as well as the presence of carbon and oxygen, are in agreement with the fact that these microcalcifications consist mainly of amorphous calcium carbonate phosphate. Magnesium and sodium are elements that can probably partially replace the calcium cations. These elements are commonly found in microcalcifications associated with aggressive forms of breast cancer [36,37]. Accordingly, some of the elements identified in these microcalcifications support the hypothesis that they may be considered indicators of malignancy [38].

3.2. Detection of psammoma bodies in the tissues using micro-FTIR spectroscopy

Psammoma bodies observed in serous ovarian carcinoma, examined by various analytical techniques, revealed very similar elemental chemical composition to that of PBs formed in papillary thyroid carcinoma [16], in line with the similarity observed by comparing the respective IR spectra. This result is worth it of consideration. In fact, while sharing common architectural alterations of the tissue (i.e., papillae with a fibro-vascular axis and presence of PBs), neoplastic cells of thyroid and ovarian are very different from a biological point of view. Thyroid carcinoma cells belong to the endocrine epithelium secreting thyroid hormones while ovarian cells derive from the epithelial lining of the ovary and fallopian tubes without hormonal function.

Exploiting this chemical similarity, a new strategy, using Micro FTIR technique, was investigated for the automated detection of such microcalcifications in unknown ovary and thyroid tissues.

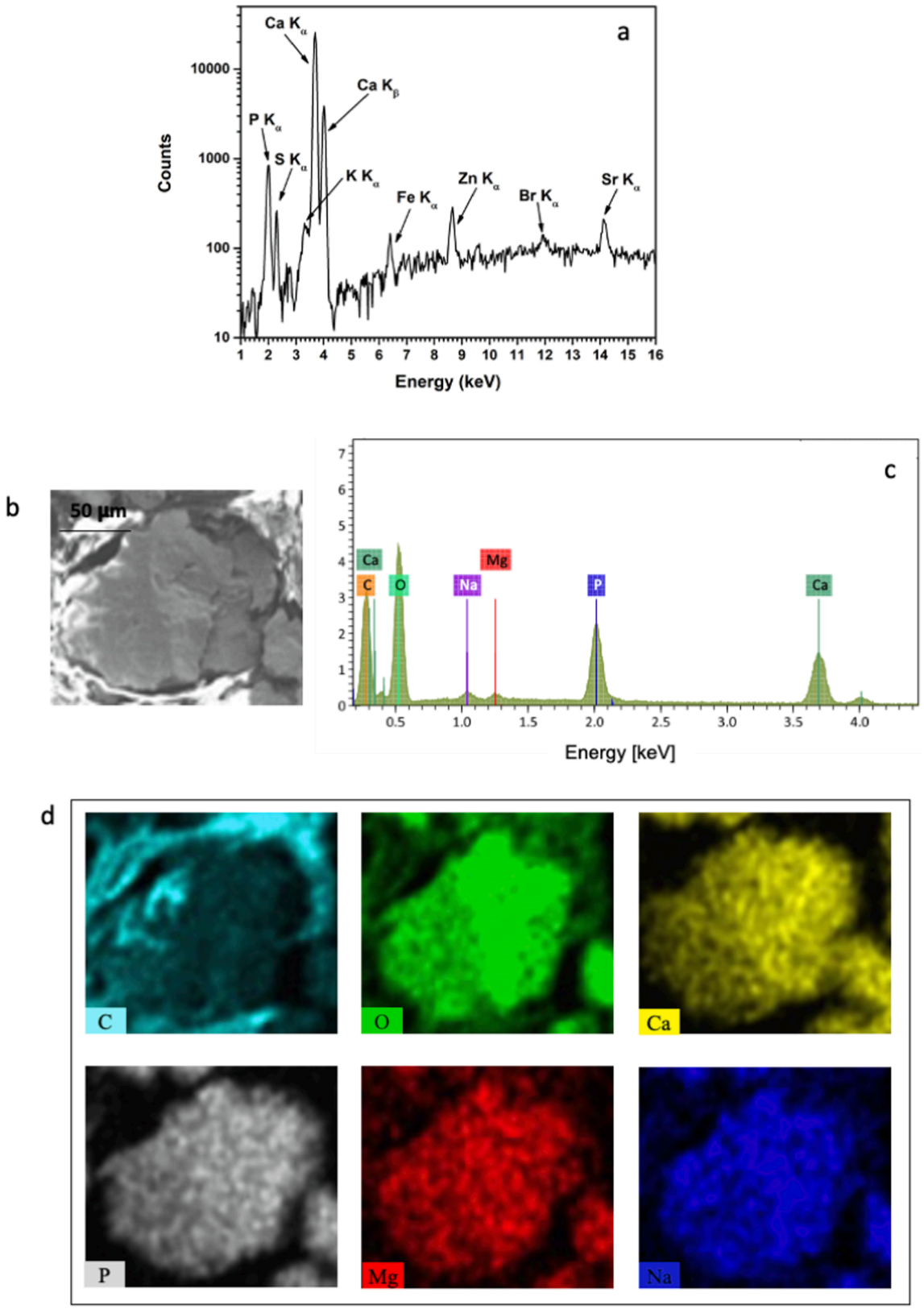

Fig. 2. (a) Representative X-ray fluorescence (XRF) spectrum: contributions of P (Kα = 2.0 keV), S (K α = 2.3 keV), K (K α = 3.3 keV), Ca (K α = 3.7 keV, Kβ = 4.0 keV), Fe (K α = 6.4 keV), Zn (K α = 8.6 keV), Br (K α = 11.9 keV) and Sr (K α = 14.1 keV). (b) SEM image and (c) EDX spectrum of a psammoma body in a slice of serousovarian carcinoma; (d) EDX maps for carbon, oxygen, sodium, phosphorous, calcium and magnesium.

3.2.1. Clustering and principal component analysis

Fuzzy C-means clustering (FCM) was chosen to determine the spectral signatures that distinguish the various tissue components, and to construct digitally colored images. In FCM a spectrum can contribute to more than one cluster depending on its degree of similarity, and the clustering images obtained correspond to the number of clusters set. This approach maximizes the use of all the information contained in each spectrum and allows for the detection and analysis of slight changes at the molecular level in each region.

FCM was applied to the spectral data in the range of 800–1800 cm^{-1} recorded from the tissue samples of high grade serous ovarian carcinoma and the corresponding digital-colored images are obtained (Fig. 3). To highlight the presence of psammoma bodies in the analyzed tissue (Fig. 3a), the choice of two clusters was sufficient, one corresponding to the inorganic material of calcifications (Fig. 3, cluster 1) and the other associated with the various organic structures of tissues (Fig. 3, cluster 2). In the cluster 1 image the red pixels are related to spectra containing mainly the signals of amorphous calcium carbonate phosphate while in the cluster 2 image the red pixels correspond to organic tissue. This analytical approach was used for another tissue sample and the digital clustering images are reported in Figure S3.

The spectra with a percentage of participation equal to or greater than 0.8 of cluster 1 and cluster 2 respectively were extracted and the corresponding average spectrum was obtained. Comparison of the second derivative of both average spectra in the 800–1100 cm^{-1} range (interval with signals related to microcalcifications) showed that the significant differences are due to the signals of the vibrational modes of phosphate and carbonate. In fact, these bands are evident in the average spectrum of the macrocalcifications (cluster 1) and in particular the carbonate signal at 870 cm^{-1} is absent in the average spectrum related to the organic tissue (Fig. 4).

Principal Component Analysis was also computed on pre-processed spectra and results obtained for the specimen subjected to clustering analysis in Fig. 3 are represented as false colored maps of scores values in Fig. 5. Scores on PC1 (Fig. 5a) show a net segregation between microcalcification patterns (red pixel) and organic environment (blue pixel), while PC2 (Fig. 5b) does not give additional information, meaning that the variance explained by PC1 is sufficient to distinguish inorganic form organic patterns. Considering the loading plot (Fig. 5c), the importance of CO_3^{2-} signal at 871 cm^{-1} in discriminating between organic and inorganic component already seen with cluster analysis is further confirmed.

3.2.2. Partial-least-square discriminant analysis (PLS-DA): Psammoma bodies detection in unknown ovarian and thyroid samples

The classification of spectral data obtained from tissue samples by clustering analysis is completely unsupervised. This method has the advantage of highlighting the natural separation between the spectra of different tissue components. Nevertheless, it is not optimized to perform a specific classification. Thus, in order to apply the infrared spectral imaging as an automated diagnostic tool, the use of Partial-Least-Square discriminant analysis, a supervised classification approach, was evaluated.

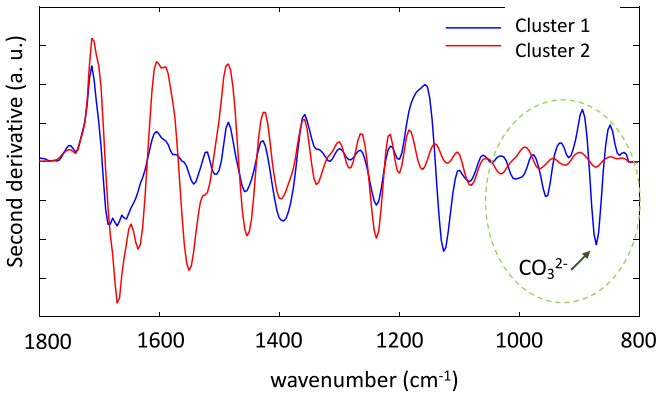

Fig. 4. Second derivates of the average spectrum associated with Cluster 1 (blue) and Cluster 2 (red). In the second derivative related to the psammoma bodies (Cluster 1) the signal of CO_3^{2-} is highlighted.

As shown above, the chemical composition of PBs in ovarian carcinoma is similar to that of PBs in thyroid carcinoma. This made it possible to evaluate the PLS-DA classification method on spectral data obtained from ovarian and thyroid tissues. The aim was to develop a single automated method to investigate the presence of these microcalcifications in the two different tissues.

The PLS-DA based prediction model was constructed using samples from two patients diagnosed with high-grade ovarian cancer, previously analyzed by Fuzzy C-means clustering (Fig. 3 and Fig. S3). These spectral data were used as the training set to build the recognition model. The accuracy of the model in internal validation was assessed from a confusion matrix (Fig. S4), which showed an excellent agreement between the real and the predicted classes. The prediction model was then applied to classify the spectral data of unknown samples. Several different tissue samples from high, low and borderline grade serous ovarian carcinoma and papillary thyroid carcinoma tissues were submitted to tissue component classifier to detect the presence of psammoma bodies.

Results of the classification were reported as chemical color-coded images in which each color corresponds to a tissue component. Pale green pixels have been assigned to psammoma bodies, dark red to organic tissue structures and blue pixels have been associated with holes (tissue-free regions generated during sample preparation) (Fig. 6, Fig. S5-S8). The reconstructed color-coded images, for each of the samples analyzed, showed good agreement with the unstained optical microscope images.

Further proof of the validity of the classification was established by

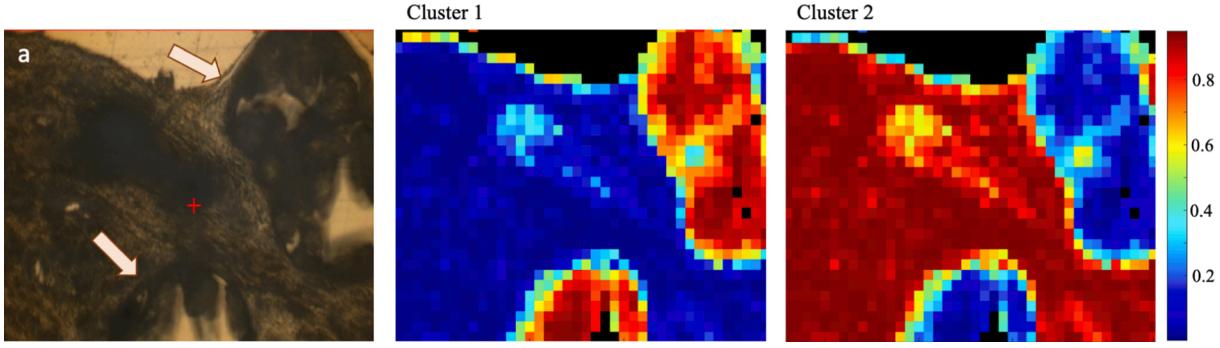

Fig. 3. FTIR light microscope images of ovarian cancer tissue of high grade with psammoma bodies (a) and the corresponding colored Fuzzy C-means images using two clusters to distinguish between psammoma bodies (cluster 1) and surrounding organic tissue (cluster 2).

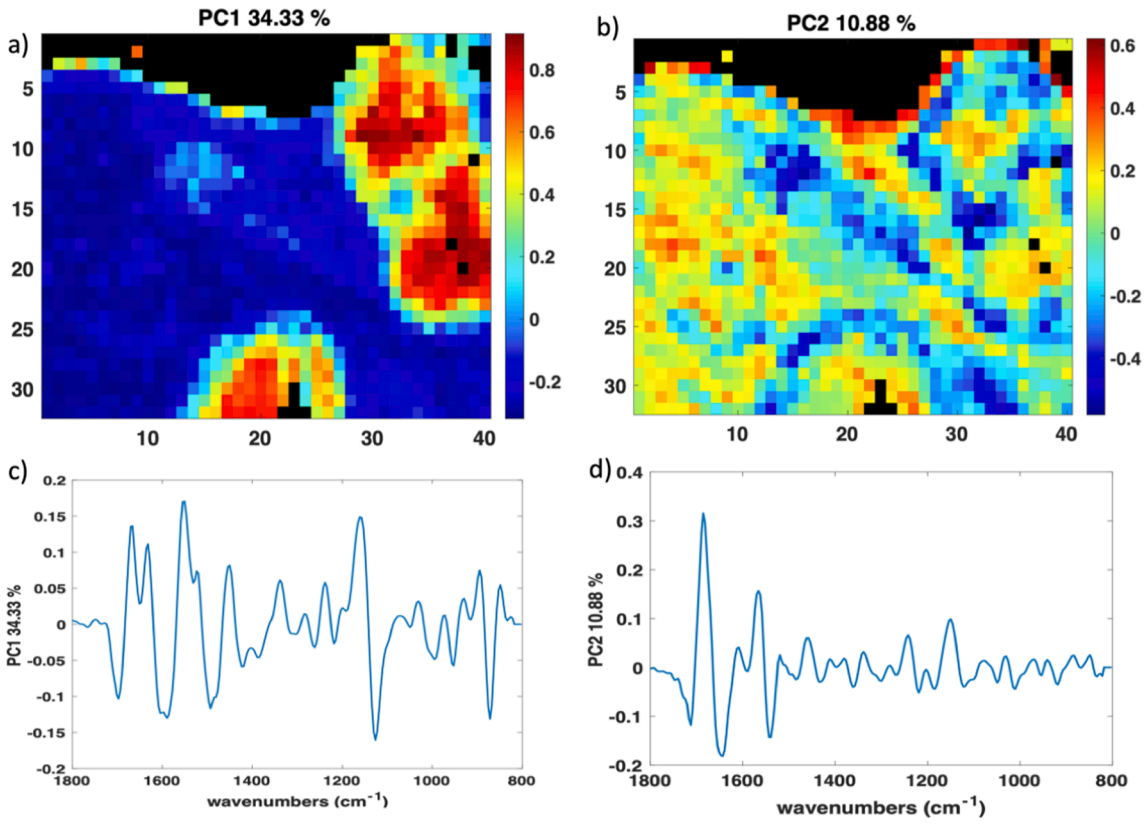

Fig. 5. PC1(a) and PC2 (b) computed on spectra recorded from high grade tissue with psammoma bodies; the corresponding loading plots are shown in c) and d), respectively.

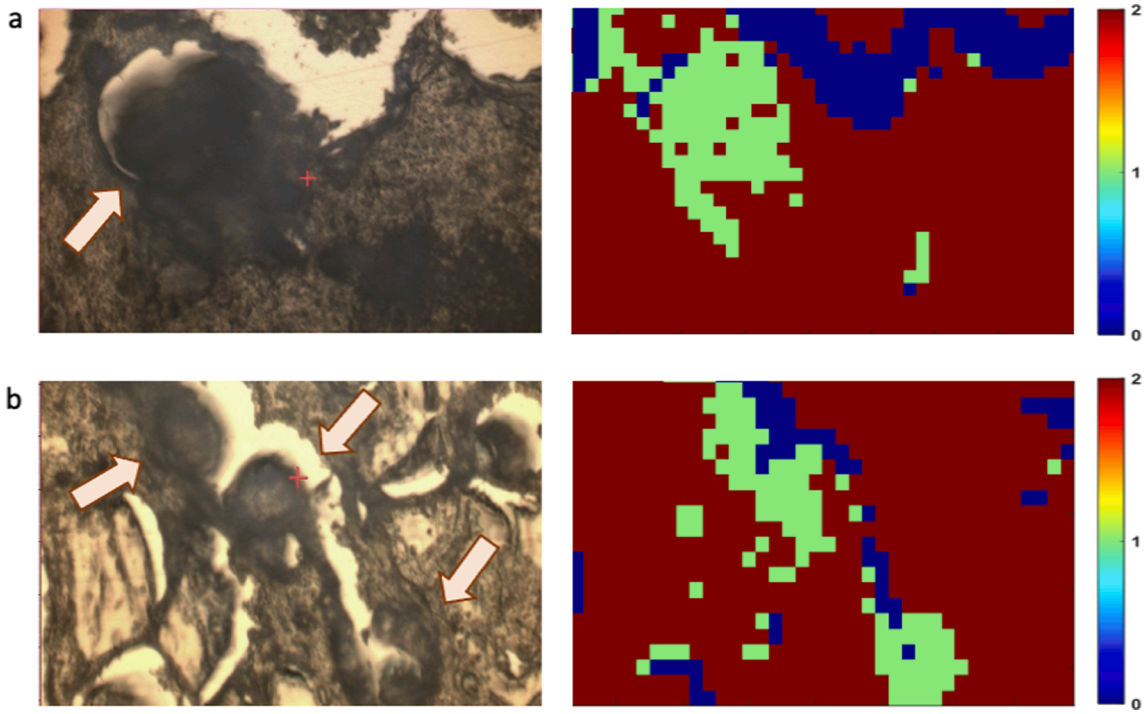

Fig. 6. FTIR light microscope images of high-grade ovarian cancer tissue (a) and thyroid cancer tissue (b) and the corresponding chemical color-coded images obtained by application of recognition PLS-DA model. Pale green identifies the psammoma bodies, dark red the organic tissue structures and blue the tissue-free zones.

comparing the second derivative of the mean spectrum of the elements assigned to the class 1 related to psammoma bodies and that of the mean spectrum of the elements associated with the rest of the organic tissue (class 2). This comparison in the range of 800–1100 cm^{-1} showed that the derivative of the mean spectrum related to class 1 reported the typical signal due to CO_3^{2-} stretching, absent in the second derivative of the mean spectrum related to class 2 (Fig. S9). This was verified in all analyzed samples.

Thus, the prediction model is found to be accurate, sensitive and specific for an automated recognition of psammoma bodies in ovarian and thyroid tissues. Moreover, with regard to ovarian tissues, detection of these microcalcifications can be done for any grade of tumor.

This automated histological detection, based only on intrinsic chemical differences of tissue components, can become a robust and unambiguous complementary tool for histopathological examinations.

4. Conclusions

The chemical content of psammoma bodies found in surgically removed human ovarian tissues of serous high-grade carcinoma, was investigated. PBs isolated from tissues were analyzed using Micro Fourier Transform Infrared Spectroscopy. It was observed that microcalcifications are composed of amorphous calcium carbonate phosphate. Moreover, some PBs grains contains phospholipids. This result could support the recently reported hypothesis that ovarian cancer cells switch to a calcifying phenotype and induce calcification, in which matrix vesicles containing lipids are the site of mineralization.

Using XRF, ICP-OES and SEM-EDX the elements contained in ovary psammoma bodies were detected. These analyses confirmed the presence of calcium and phosphate and revealed that Fe, Zn, Cu, Na and Mg can be found in these formations. The presence of iron, zinc and copper is in agreement with other studies which observed increased amounts of these elements during tumor progression. In addition, sodium and magnesium were observed in other malignant tumor microcalcifications. These results support the idea that some elements can be considered indicators of malignancy.

These results made it possible to state that PBs, found in ovarian serous tumors, show a composition comparable to that of PBs isolated from papillary thyroid carcinoma analyzed in previous works. Starting from chemical similarities between IR spectra of PBs from the two different tissues, an automated recognition method was constructed. Such predictive model allowed detection of PB on unknown tissue samples of ovarian carcinoma of different grades (high, low and borderline) and thyroid carcinoma with good sensitivity. This approach could become a routine method of investigation to support morphological assessment, because it does not require specimen staining and overcomes the subjectivity of conventional histopathological analysis.

CRediT authorship contribution statement

Francesco Porcelli: Conceptualization, Validation, Investigation, Writing – original draft, Writing – review & editing. **Martina Verri:** Conceptualization, Validation, Investigation, Formal analysis, Writing – original draft, Writing – review & editing. **Serena De Santis:** Conceptualization, Validation, Investigation, Formal analysis, Writing – original draft, Writing – review & editing. **Anna Crescenzi:** Investigation, Resources, Writing – review & editing. **Antonella Bianchi:** Investigation, Resources, Writing – review & editing. **Anna Candida Felici:** Investigation, Formal analysis. **Giovanni Sotgiu:** Investigation, Resources, Formal analysis, Writing – review & editing. **Susanna Romano:** Investigation, Formal analysis. **Monica Orsini:** Conceptualization, Validation, Investigation, Writing – original draft, Writing – review & editing, Supervision.

Declaration of Competing Interest

The authors declare that they have no known competing financial interests or personal relationships that could have appeared to influence the work reported in this paper.

Acknowledgement

Dr. Giuseppe Rizzitelli, CIANA s.r.l. for ICP analysis.

Appendix A. Supplementary material

Supplementary data to this article can be found online at https://doi.org/10.1016/j.saa.2023.122792.

References

[1] D. Proudfoot, Calcium signaling and tissue calcification, Cold Spring Harb. Perspect. Biol. 11 (2019), https://doi.org/10.1101/cshperspect.a035303.
[2] N. Vidavsky, J.A.M.R. Kunitake, L.A. Estroff, Multiple pathways for pathological calcification in the human body, Adv. Healthc. Mater. 10 (2021), https://doi.org/10.1002/adhm.202001271.
[3] D. Bazin, M. Daudon, C. Combes, C. Rey, Characterization and some physicochemical aspects of pathological microcalcifications, Chem. Rev. 112 (2012) 5092–5120, https://doi.org/10.1021/cr200068d.
[4] J.A.M.R. Kunitake, S. Choi, K.X. Nguyen, M.M. Lee, F. He, D. Sudilovsky, P. G. Morris, M.S. Jochelson, C.A. Hudis, D.A. Muller, P. Fratzl, C. Fischbach, A. Masic, L.A. Estroff, Correlative imaging reveals physiochemical heterogeneity of microcalcifications in human breast carcinomas, J. Struct. Biol. 202 (2018) 25–34, https://doi.org/10.1016/j.jsb.2017.12.002.
[5] R. Bonfiglio, A. Granaglia, R. Giocondo, M. Scimeca, E. Bonanno, Molecular aspects and prognostic significance of microcalcifications in human pathology: a narrative review, Int. J. Mol. Sci. 22 (2021) 1–14, https://doi.org/10.3390/ijms22010120.
[6] L.B. Ferreira, E. Gimba, J. Vinagre, M. Sobrinho-Simões, P. Soares, Molecular aspects of thyroid calcification, Int. J. Mol. Sci. 21 (2020) 1–20, https://doi.org/10.3390/ijms21207718.
[7] J.L. Hunt, E. Leon Barnes, Non-tumor-associated psammoma bodies in the thyroid, Am. J. Clin. Pathol. 119 (2003) 90–94, https://doi.org/10.1092/RWPPYCBYT2JVA023.
[8] L. Cardisciani, F. Policardo, P. Tralongo, V. Fiorentino, E.D. Rossi, What psammoma bodies can represent in the thyroid. What we recently learnt from a story of lack of evidence, Pathologica. 114 (2022) 373–375. https://doi.org/10.32074/1591-951X-815.
[9] N. Liu, F. Qu, K. Wei, W. Gan, Z. Wang, W. Zhuang, S. Agizamhan, W. Ma, J. Yang, M. Chen, L. Xu, H. Guo, D. Li, Incidence and significance of psammoma bodies in Xp11.2 translocation renal cell carcinoma and papillary renal cell carcinoma, Oncol. Lett. 18 (2019) 472–478, https://doi.org/10.3892/ol.2019.10305.
[10] E. Ersoy, R.M. Kashikar, Psammoma bodies in Papanicolaou tests and associated factors to predict an underlying malignancy: a clinicopathological analysis of 10 cases, J. Am. Soc. Cytopathol. 9 (2020) 266–271, https://doi.org/10.1016/j.jasc.2020.04.002.
[11] B.K. Kim, E.M. Lee, J.H. Kim, S.Y. Oak, S.K. Kwon, Y.S. Choi, Y.O. Kim, Relationship between ultrasonographic and pathologic calcification patterns in papillary thyroid cancer, Med. (United States). 97 (2018), https://doi.org/10.1097/MD.0000000000012675.
[12] S.S. Carneiro, B.W. Scheithauer, O.G. Nascimento, T. Hirose, D.H. Davis, ANATOMIC PATHOLOGY Solitary Fibrous Tumor of the Meninges: A Lesion Distinct From Fibrous Meningioma A Clinicopathologic and Immunohistochemical Study, n.d. https://academic.oup.com/ajcp/article/106/2/217/1756680.
[13] B. Sorbe, B. Frankendal, Prognostic importance of psammoma bodies in adenocarcinomas of the ovaries, Gynecol. Oncol. 14 (1982) 6–14, https://doi.org/10.1016/0090-8258(82)90045-2.
[14] D.K. Das, Psammoma body: A product of dystrophic calcification or of a biologically active process that aims at limiting the growth and spread of tumor? Diagn. Cytopathol. 37 (2009) 534–541, https://doi.org/10.1002/dc.21081.
[15] T. Kubota, T. Yamashima, M. Hasegawa, S. Kida, M. Hayashi, S. Yamamoto, Formation of psammoma bodies in meningocytic whorls, Acta Neuropathol. 70 (1986) 262–268, https://doi.org/10.1007/BF00686081.
[16] S. de Santis, G. Sotgiu, A. Crescenzi, C. Taffon, A.C. Felici, M. Orsini, On the chemical composition of psammoma bodies microcalcifications in thyroid cancer tissues, J. Pharm. Biomed. Anal. 190 (2020), https://doi.org/10.1016/j.jpba.2020.113534.
[17] S. de Santis, F. Porcelli, G. Sotgiu, A. Crescenzi, A. Ceccucci, M. Verri, M. Caricato, C. Taffon, M. Orsini, Identification of remodeled collagen fibers in tumor stroma by FTIR Micro-spectroscopy: a new approach to recognize the colon carcinoma, Biochim. Biophys. Acta Mol. basis Dis. 1868 (2022), https://doi.org/10.1016/j.bbadis.2021.166279.
[18] M.J. Baker, J. Trevisan, P. Bassan, R. Bhargava, H.J. Butler, K.M. Dorling, P. R. Fielden, S.W. Fogarty, N.J. Fullwood, K.A. Heys, C. Hughes, P. Lasch, P. L. Martin-Hirsch, B. Obinaju, G.D. Sockalingum, J. Sulé-Suso, R.J. Strong, M. J. Walsh, B.R. Wood, P. Gardner, F.L. Martin, Using Fourier transform IR

spectroscopy to analyze biological materials, Nat. Protoc. 9 (2014) 1771–1791, https://doi.org/10.1038/nprot.2014.110.
[19] WHO Classification of Tumours Editorial Board., Female genital tumours, in: WHO Classification of Tumours Series, 5th ed., International Agency for Research on Cancer, Lyon (France), 2020.
[20] WHO Classification of Tumours Editorial Board, Endocrine and neuroendocrine tumours WHO Classification of Tumours Series 5th ed., 2022 International Agency for Research on Cancer Lyon (France).
[21] A. Zancla, S. de Santis, G. Sotgiu, C. Taffon, A. Crescenzi, M. Orsini, Micro-FTIR spectroscopy as robust tool for psammoma bodies detection in papillary thyroid carcinoma, Spectrochim. Acta A Mol. Biomol. Spectrosc. 229 (2020), https://doi.org/10.1016/j.saa.2019.117984.
[22] B. Yin, J.Y. Mi, H.L. Zhai, B.Q. Zhao, K.X. Bi, An effective approach to the early diagnosis of colorectal cancer based on three-dimensional fluorescence spectra of human blood plasma, J. Pharm. Biomed. Anal. 193 (2021), https://doi.org/10.1016/j.jpba.2020.113757.
[23] M.P. Diago, J. Fernández-Novales, S. Gutiérrez, M. Marañón, J. Tardaguila, Development and validation of a new methodology to assess the vineyard water status by on-the-go near infrared spectroscopy, Front. Plant Sci. 9 (2018), https://doi.org/10.3389/fpls.2018.00059.
[24] D. Ballabio, V. Consonni, Classification tools in chemistry. Part 1: Linear models. PLS-DA, Anal. Methods 5 (2013) 3790–3798, https://doi.org/10.1039/c3ay40582f.
[25] Y. Li, F. Kong, W. Weng, Preparation and characterization of novel biphasic calcium phosphate powders (α-TCP/HA) derived from carbonated amorphous calcium phosphates, J. Biomed. Mater. Res. B Appl. Biomater. 89 (2009) 508–517, https://doi.org/10.1002/jbm.b.31242.
[26] M.E. Fleet, Infrared spectra of carbonate apatites: ν2-Region bands, Biomaterials 30 (2009) 1473–1481, https://doi.org/10.1016/j.biomaterials.2008.12.007.
[27] Y. Zhang, C. Wang, Y. Li, A. Lu, F. Meng, H. Ding, F. Mei, J. Liu, K. Li, C. Yang, J. Du, Y. Li, Carbonate and cation substitutions in hydroxylapatite in breast cancer micro-calcifications, Mineral. Mag. 85 (2021) 321–331, https://doi.org/10.1180/mgm.2021.23.
[28] M. Fanlu, W. Changqiu, L. Yan, L. Anhuai, M. Fang, L. Jianying, D. Jingyun, Z. Yan, Psammoma bodies in two types of human ovarian tumours: a mineralogical study, Mineral. Petrol. 109 (2015) 357–365, https://doi.org/10.1007/s00710-014-0342-6.
[29] R.N.A.H. Lewis, R.N. McElhaney, The structure and organization of phospholipid bilayers as revealed by infrared spectroscopy, Chem. Phys. Lipids 96 (1998) 9–21, https://doi.org/10.1016/S0009-3084(98)00077-2.
[30] A. Cernescu, M. Szuwarzyński, U. Kwolek, P. Wydro, M. Kepczynski, S. Zapotoczny, M. Nowakowska, L. Quaroni, Label-free infrared spectroscopy and imaging of single phospholipid bilayers with nanoscale resolution, Anal. Chem. 90 (2018) 10179–10186, https://doi.org/10.1021/acs.analchem.8b00485.
[31] L. Jing, L. Li, Z. Sun, Z. Bao, C. Shao, J. Yan, Q. Pang, Y. Geng, L. Zhang, X. Wang, Z. Wang, Role of matrix vesicles in bone-vascular cross-talk, J. Cardiovasc. Pharmacol. 74 (2019) 372–378, https://doi.org/10.1097/FJC.0000000000000720.
[32] J. Wen, Z. Zhao, L. Huang, L. Li, J. Li, Y. Zeng, J. Wu, Y. Miao, Switch of the ovarian cancer cell to a calcifying phenotype in the calcification of ovarian cancer, J. Cancer 9 (2018) 1006–1016, https://doi.org/10.7150/jca.22932.
[33] S. Zhao, X. Zhang, F. Gao, H. Chi, J. Zhang, Z. Xia, C. Cheng, J. Liu, Identification of copper metabolism-related subtypes and establishment of the prognostic model in ovarian cancer, Front Endocrinol (Lausanne). 14 (2023), https://doi.org/10.3389/fendo.2023.1145797.
[34] M. Jung, C. Mertens, E. Tomat, B. Brüne, Iron as a central player and promising target in cancer progression, Int. J. Mol. Sci. 20 (2019), https://doi.org/10.3390/ijms20020273.
[35] K. Michalczyk, A. Cymbaluk-Płoska, The role of zinc and copper in gynecological malignancies, Nutrients 12 (2020) 1–21, https://doi.org/10.3390/nu12123732.
[36] M. Scimeca, E. Giannini, C. Antonacci, C.A. Pistolese, L.G. Spagnoli, E. Bonanno, Microcalcifications in breast cancer: an active phenomenon mediated by epithelial cells with mesenchymal characteristics, BMC Cancer 14 (2014), https://doi.org/10.1186/1471-2407-14-286.
[37] R. Scott, C. Kendall, N. Stone, K. Rogers, Elemental vs. phase composition of breast calcifications, Sci. Rep. 7 (2017), https://doi.org/10.1038/s41598-017-00183-y.
[38] L. Gotnayer, D. Aranovich, M. Fraenkel, U. Yoel, N. Vidavsky, Zinc in microscopic calcifications isolated from thyroid fine needle aspiration may serve as a biomarker of thyroid nodule malignancy: a promising proof-of-concept, Acta Biomater. (2023), https://doi.org/10.1016/j.actbio.2023.03.010.